



# Modelization and implementation of free adsorption and electrosorption of Cr (VI) from wastewater using Al<sub>2</sub>O<sub>3</sub> nanoparticles: assessment and comparison of the two processes

Wafa Sassi<sup>1,2</sup> · Hana Boubaker<sup>3</sup> · Hayet Ben-khaled<sup>1</sup> · Sana Dhaoui<sup>1</sup> · Achraf Ghorbal<sup>1,3</sup> · Jean-Yves Hihn<sup>4</sup>

Received: 14 October 2020 / Accepted: 18 January 2021 / Published online: 4 February 2021  
© The Author(s), under exclusive licence to Springer-Verlag GmbH, DE part of Springer Nature 2021

## Abstract

The objective of this study was to apply the technique of electrosorption in order to assess the capacity of heterogeneous adsorption under an electric field. This was to enhance the adsorption capacity of the nanoparticles, to shorten the adsorption time, and to reduce the cost of the purification of contaminated waters. A final objective of this study was to compare the free adsorption (FA) and the electrosorption (ES) to understand the interface adsorbent/adsorbate at different contact conditions. For these purposes, a potentially efficient, environment-friendly adsorbent was synthesized for dechromation purposes. The experimental design method generated optimum conditions as  $t_c = 123$  min,  $T = 318^\circ\text{K}$ , and  $C_0 = 100$  mg/L. Freundlich's well-fitted modeling proved that the adsorption of chromate (VI) on nano-Al<sub>2</sub>O<sub>3</sub> occurred on a homogenous surface. In addition, the adsorption coefficient intensity  $n$  did not only confirm monolayer adsorption but also indicated a favorable adsorption process. Thermodynamic studies confirmed the reaction spontaneity and the physisorption of the process. The electrosorption process was also tested using 20mA/cm<sup>2</sup> as applied current density. Free-adsorption (FA) and electrosorption (ES) processes were compared. The maximum recorded yield was 99% for (EA) against 87% for (FA). EDS analysis recorded 11.3% of chromate adsorbate with free adsorption. The amount of Cr (VI) on nano-Al<sub>2</sub>O<sub>3</sub> was 42.5 %. Nevertheless, the Al<sub>2</sub>O<sub>3</sub> nanoparticles lost their crystallinity and exploded after the ES process. Mechanisms of both (FA) and (ES) were proposed.

**Keywords** Adsorption · Electrosorption · Nano-Al<sub>2</sub>O<sub>3</sub> · Cr (VI) · Isotherms

## Introduction

One of the most dangerous industrial wastes is chromate (Cr) since it is highly toxic even at low concentrations and harmful to

human health. It was identified as a serious cause of diseases such as cancer, kidney damage, and nervous system damage. In addition, Thabede et al. (2020) classified Cr as a harmful pollutant for the environment and living beings. For this reason, research has focused on ways and techniques for ridding the environment of this hazardous element. The main devised processes for this purpose were simple and spontaneous like precipitation, adsorption, and absorption or artificial-like electrocoagulation, photodegradation, and catalysis. Xing et al. (2021), Ighalo et al. (2020), and Soliman and Moustafa (2020) observed that spontaneous adsorption was the most commonly used process for industry al wastewater treatment. However, the choice of the right process depended on the required quality and the non-toxicity of the adsorbent. Hence, the treatment methods and approaches abounded for the elimination of the toxic Cr (VI). Thabede et al. (2020) tried the adsorption of Cr (VI). Yadav and Bhattacharyya (2019) attempted the electrochemical method. Mor et al. (2007) tried co-precipitation. Diao et al. (2017) reported on photocatalysis. Cai et al. (2009) adopted the coagulation process. Bharath et al. (2019) implemented peanut shell/Fe<sub>3</sub>O<sub>4</sub>

Responsible Editor: Ioannis A. Katsoyiannis

✉ Wafa Sassi  
wafa.sassi@issatgb.u-gabes.tn

- <sup>1</sup> Higher Institute of Applied Sciences and Technology of Gabes, Gabes University, Avenue Omar Ibn El Khattab, 6029 Gabes, Tunisia
- <sup>2</sup> Unité de Recherche Electrochimie, Matériaux et Environnement UREME (UR17ES45), Faculté des Sciences de Gabès, Université de Gabès, Cité Erriadh, 6072 Gabès, Tunisia
- <sup>3</sup> Research Laboratory LR18ES33, National Engineering School of Gabes, University of Gabes, Avenue Omar Ibn El Khattab, 6029 Gabès, Tunisia
- <sup>4</sup> Institut UTINAM, CNRS UMR 6213, Univ Bourgogne Franche-Comté, 16 route de Gray, 25030 Besançon Cedex, France

nanocomposite and  $\text{Ti}_3\text{AlC}_2$ /porous graphene asymmetric electrodes. More recently, these scholars applied the electrochemical performances of some innovative electrodes for the capacitive deionization Cr (VI) ions by fabricated activated carbon (Bharath et al. 2020). Mourtah et al. opted for the membrane procedure. Within this approach, Lin et al. (2020) used membranes from rice straws for the separation of the contaminants Chu et al. (2020) eliminated Cr (VI) by membranes from activated carbon. Chowdhury et al. (2018) designed membranes from nanocomposites for the removal of Cr (VI).

In particular, Tian et al. (2016) recommend  $\text{Al}_2\text{O}_3$  as a very adequate material for making separation membranes. These scholars reported that its porous hollow microspheres, its chemical stability in the environment, its hardness, and its excellent performance in the adsorption of organic dyes designed it as the right choice for water treatment. In addition, Lin et al. (2020), Amalraj and Michael (2019), and Mohammed et al. (2020) observed that its resistance to corrosion was an extra advantage for its use in various fields such as in biomedical applications, photovoltaic applications, and water boiler fabrication. Nevertheless, despite these advantages, the use of  $\text{Al}_2\text{O}_3$  in separation membranes showed a serious shortcoming because its adsorption rate proved to be time-consuming. Consequently, researchers such as Gaikwad and Balomajumder (2018) thought of implementing the electrosorption technique. They reported that this was a simple process that was much more economical than its predecessors. In addition, it showed a high removal yield. 3.227 mg/g of Cr (VI) and 2.775 mg/g of fluoride are uptaken using biomass electrode. Using a biomass electrode, these scholars succeeded in removing 3.227 mg/g of Cr (VI) and 2.775 mg/g of fluoride. More recently, Gaikwad et al. (2020) used a novel acid-treated (RHWBAC) electrode. They succeeded in removing 2.8316 mg/g of Cr (VI). Nevertheless, to our knowledge, no research has yet attempted to show the capacity of heterogeneous adsorption under an electric field.

For this reason, this study purported to join this trend of research and contribute the novelty of applying the technique of electrosorption in order to assess the capacity of heterogeneous adsorption under an electric field. The ultimate objective would be to enhance the adsorption capacity of the nanoparticles, to shorten the adsorption time, and to reduce the cost of the purification of contaminated waters. A final objective of this study was to compare the free adsorption (FA) and the electrosorption (ES) to understand the interface adsorbent/adsorbate at different contact conditions.

## Methods and instruments

### Apparatus

The ultra-violet spectrophotometer used in this paper was described elsewhere (Karoui et al. 2020). A high-resolution

compact SEM third generation from HITACHI and model FlexSEM1000 II and energy-dispersive spectroscopy (EDS, Oxford instrument EDS Aztec, Wiesbaden, UK) were used to investigate the elemental analysis of samples (Sassi et al., 2020a, b, c). Therefore, the samples were filtered, dried at 323°K for 2 h to eliminate humidity, and conserved in a desiccator for 3 h before SEM analysis. The recovered  $\text{Al}_2\text{O}_3$  nanoparticles were spread on a non-interactive glassy slide for better visualization. For empirical comparison, the raw nanoparticles and the samples were treated in the same conditions. They were stirred into water at the optimum conditions of acidity (pH), temperature (T), and contact time (tc). Then, they were filtered, washed, and dried. The preferred orientations of the obtained nanoparticles were determined by X-ray diffraction under shaving incidence (XRD-Ras) using a D8 advance Bruker (with Bragg–Bretano configuration) with Cu-K $\alpha$  radiation ( $\lambda = 1.54060 \text{ \AA}$ ). The  $2\theta$  range of 30 to 95° was recorded at a rate of  $0.02^\circ \text{ s}^{-1}$  as was reported by Sassi et al. (Sassi et al., 2020a, b, c).

### Synthesis of $\text{Al}_2\text{O}_3$ nanoparticles

Following Baba et al. (2020), Balyan et al. (2020), Abbas-Ghaleb et al. (2019), and El-Nahas et al. (2019), many tests were conducted but only the following experiment was retained. All used chemicals were from Sigma-Aldrich with no less than, at least, or with 99% purity. Firstly, 0.156 moles of alumina chloride powder were dissolved in 170 mL of hydrochloride acid with a concentration of 1.5 M. After stirring for 2 min, the liquid was poured into a beaker containing 0.312 moles of acetone. The mixture was diluted with 3 l of distilled water. Then, the system was bombarded for 2 h by pure oxygen. After rapid adding of 300 ml of ammonia and stirring very hard at room temperature (about 293°K), the  $\text{Al}_2\text{O}_3$  oxides precipitated. After decantation, alumina flakes appeared at the bottom and the supernatant was discarded

Secondly, drying/washing cycles were applied in order to eliminate ammoniac and acetone from the solid nanoparticles. After drying, the nanoparticles were soaked in the distilled water under agitation, then filtered and dried. The drying/washing cycles were interrupted when the filtered water recorded a neutral pH (about 7). The nanoparticles of  $\text{Al}_2\text{O}_3$  were calcinated at 1273°K for 2 h. The alumina was ground and sieved after drying to obtain similar spherical nanoparticles.

Fig. 1 shows the SEM, EDS, and XRD analyses of the obtained raw alumina nanoparticles.

A close observation of Fig. 1A would reveal that the nano- $\text{Al}_2\text{O}_3$  particles were homogeneous in shape and measured about 30 nm each. The EDS spectra in Fig. 1B would prove the purity of the nanoparticles. The XRD spectra in Fig. 1C would confirm the crystallinity of the obtained nanoparticles. In addition, this would confirm Lamouri et al.'s (2017)

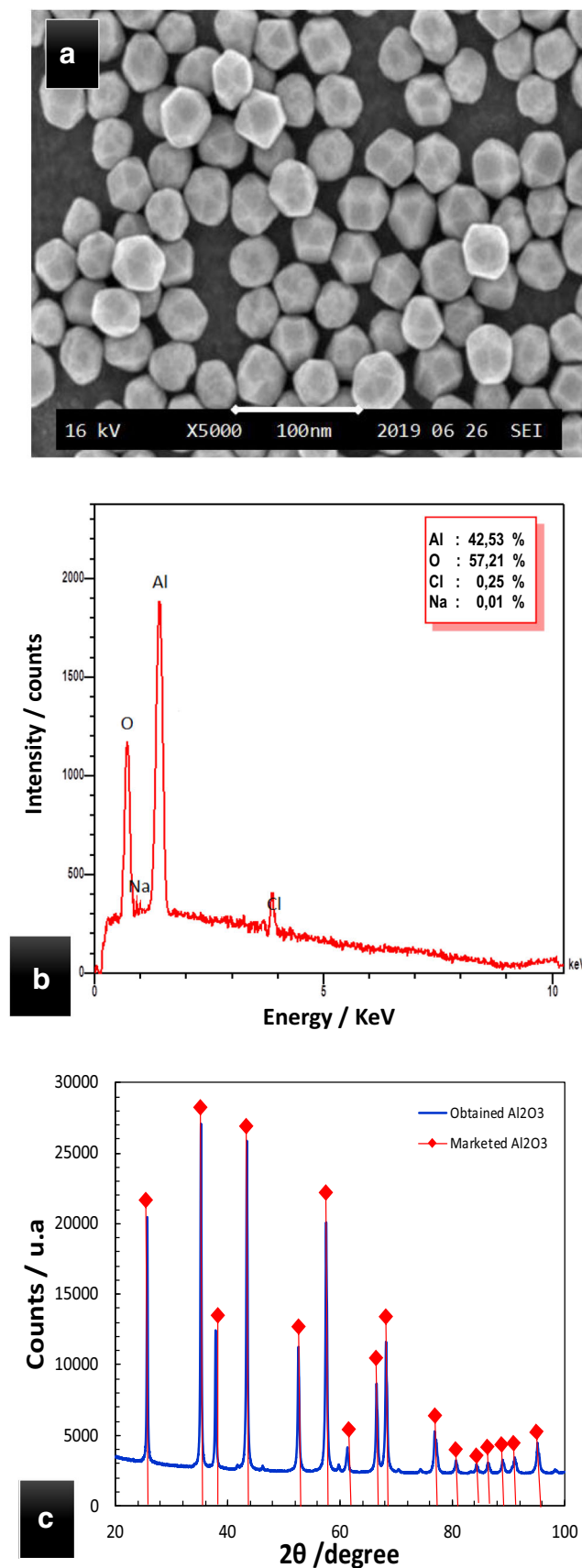


**Fig. 1** (A) SEM micrographs, (B) EDS spectra, and (C) XRD spectra of the obtained dried Al<sub>2</sub>O<sub>3</sub> nanoparticles

observation about the presence of the  $\alpha$  phase commonly known as the corundum.

### Adsorbate and reagents

The engineered wastewater was set up with distilled water and potassium dichromate (Cr (VI)). The contaminant element was K<sub>2</sub>CrO<sub>7</sub> and acquired from Sigma-Aldrich. The detection of Cr (VI) was realized by a UV-visible spectrophotometer. Standards, UV-visible spectrum, and a calibration curve of the prepared adsorbate chromate (VI) were presented in [supplementary data](#).

### Determination of the pH<sub>pzc</sub> parameter

The pH of point zero charge is an interesting value of pH which reflects the evolution of the surface charge of the nanoparticle in function of the pH of its environment. The nanoparticles (0.01g) were put into 100 mL of NaCl solution (0.01 M) at different pH<sub>initial</sub> (2–12), stirred at 250 rpm, and stored at room temperature. After 24h, the pH<sub>final</sub> of the solution was measured.

### Electrochemical study

The experiment was conducted into a classic electrochemical reactor (shown in [supplementary data](#)). It was connected to an Autolab Generator from Metrohm potentiostat-galvanostat, reference AUTOLABPGSTAT302N. The system was piloted by NOVA 2.1.4 software 2019 edition. It was used for cyclic voltammetry analysis and chronopotentiometry methods. The electrochemical reactor was a three-electrode cell. An Ag/AgCl electrode (Argenthal, 3 M KCl, 0.207V vs. SHE at 298°K) was used as the reference electrode (RE). Two thin rods of platinum with an exposed area of 1cm<sup>2</sup> surface were employed as the counter (CE) and the work (WE) electrodes. The space between the electrodes was a 1-cm constant distance. The electrolyte temperature was controlled with a thermostat. All tests were repeated 3 times to have reproducibility.

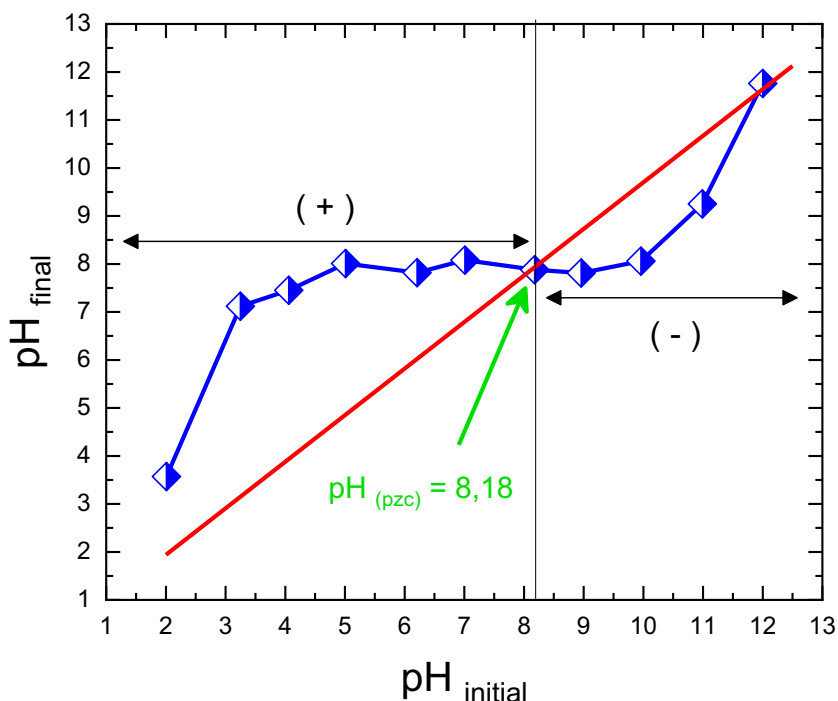
## Results and discussion

### The pH<sub>pzc</sub> parameter

Figure 2 exhibits the pH<sub>final</sub> curve in function of pH<sub>initial</sub>.

The pH<sub>pzc</sub> is the pH of zero superficial charge value when pH<sub>initial</sub> is equal to pH<sub>final</sub>. Figure 2 shows the evolution of pH<sub>final</sub> function of pH<sub>initial</sub> of the nano-Al<sub>2</sub>O<sub>3</sub>. The pH<sub>pzc</sub> of Al<sub>2</sub>O<sub>3</sub> nanoparticles was 8.18. When pH was less than pH<sub>pzc</sub>, the adsorbent surface was positively charged, and the adsorption of anions was favored as was shown by Karoui et al. (Karoui et al. 2020). However, if pH was greater than pH<sub>pzc</sub>,

**Fig. 2** Evolution of  $pH_{final}$  function of  $pH_{initial}$  of the nano- $Al_2O_3$



the adsorbent surface was negatively charged, and adsorption of cations was favored. The contaminant in this study was the Cr hexavalent but under its anionic oxide form  $Cr_2O_7^{2-}$ . Therefore, the most preferable adsorption of alumina would be in the acid pH area and especially at  $pH = 3.5$ .

**Central composite design optimization**

The simulation model and error analysis are presented in a [supplementary data file](#). Firstly, the adsorption of the chromate on alumina nanoparticles was analyzed with STATISTICA 12.8.0 software and optimized using the CCD model and response surface methodology (RSM). The purpose of the study was to obtain the optimum conditions of some studied factors. The RSM based on the CCD would allow to minimize the number of experiments as was reported by Diao et al. (2017). The effect of all studied factors and the interaction between them on the response ( $Y\%$ : adsorption yield) were calculated using CCD as was recommended by Diao et al. (2017) and Pils and Laird (2007). The adsorption yield was calculated using Eq. 1:

$$\%Y = \frac{C_0 - C_f}{C_0} \times 100 \tag{1}$$

where  $C_0$  and  $C_f$  are the initial concentration and the residual concentrations after adsorption, respectively, of the chromate into the media. This percentage of removal of Cr (VI) from synthesized wastewater seemed to depend on 4 principal factors namely contact time ( $t_c$ /min), temperature ( $T$ /°K), and

concentration of the pollutant ( $C$ /mg/L). Table 1 presents the experimental domain and codes for each factor.

Several scholars agreed that the chosen interval values for each factor had a great impact on the adsorption yield of Cr on nano- $Al_2O_3$  (Li et al. 2017; Wan et al. 2019; Zhang et al. 2019, 2020; Luo et al. 2020; Qiu et al. 2020).

The experimental design generated by the software and the percentage of elimination yield are presented in Table 2.

The experimental design in Table 2 shows that the experimental domain of each factor was successful. Indeed, the adsorption seemed to have happened and recorded a yield percentage ranging from 8 to 81%. It should be noted that for experiment 8, conducted with 150 mg/L of pollutant concentration at a temperature of 343°K and a  $t_c$  of up to 180 min, there was a quasi-absence of adsorption of only 00.3%.

The mathematical prediction model generated by the software yielded two main results, namely, the equation predicting any future experience in this field (Eq. 2) and the correlation between predicted and experimental yield values (Fig. 3).

**Table 1** Experimental domain and codes for each factor

Factor	Code	Low value	Center	High value
$t_c$ (min)	$X_1$	1	720.5	1440
$T$ (°K)	$X_2$	293	318	343
$C$ (mg/L)	$X_3$	50	100	150

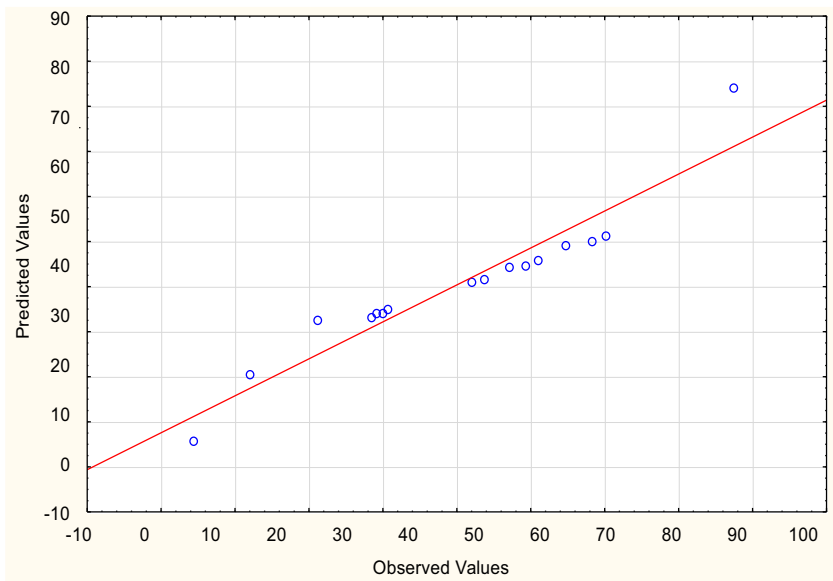
**Table 2** Experimental design and responses

No. exp.	$t_c$ (min)	$T$ (°K)	$C$ (mg/L)	Yield (%)
1	10	293	50	26.3
2	10	293	150	44.2
3	10	343	50	78.2
4	10	343	150	45.6
5	180	293	50	71.3
6	180	293	150	23.6
7	180	343	50	12.2
8	180	343	150	00.3
9	1	318	100	08.7
10	237.9	318	100	58.4
11	95	275.6	100	79.3
12	95	360.4	100	81.4
13	95	318	15.9	55.6
14	95	318	184.1	12.3
15	95	318	100	12.8
16	95	318	100	12.6

$$\begin{aligned}
 Y_1 = & (8.976) + (-0.929 \times X_1) + (-2.879 \times X_2) \\
 & + (-21.425 \times X_3) + (-33.788 \times X_1X_2) \\
 & + (-11.327 \times X_1X_3) + (-3.819 \times X_2X_3) \\
 & + (0,687 \times X_1X_2X_3) + 0,18 \tag{2}
 \end{aligned}$$

The effect weight of each factor was interpreted by the coefficient value and sign. Indeed, the third factor  $X_3$  (concentration of the pollutant) had the highest effect on the adsorption yield but this effect was inversely proportional since

**Fig. 3** Observed versus predicted values of dependent variable (%Y) for chromates removal with  $Al_2O_3$  nanoparticles



the coefficient was negative. Since the experimental points were close to the theoretical line (Fig. 3), the recording of 0.18% as residual value of predicted adsorption percentage (Eq. 2) and the non-linear regression coefficient was  $R^2 = 0.9402$ , then the simulated model would be acceptable.

Figure 4 shows the profiles for the desirability function (DF) option and the predicted values to determine the optimum conditions for the adsorption process. The scale from 0 (undesirable) to 1 (highly desirable) would provide the global function that had to be maximized based on an efficient choice and optimization of the independent variables. The desirability of 0.5 would correspond to the mean adsorption percentage as was revealed by Karoui et al. (2020). The optimum conditions generated by the software are presented in Fig. 4. They were  $t_c = 123$  min,  $T = 318^\circ K$ , and  $C_r$  concentration = 100 mg/L. These optimum conditions were adopted for all the subsequent tests. The DF predicted an adsorption yield range from 0.33 to around 87%. This removal percentage of chromate using  $Al_2O_3$  nanoparticles was clearly higher than that reported in previous works using spontaneous adsorption on activated alumina. Indeed, Lee et al. (2014) reached only the adsorption of 26% of Fluor. Finally, Cai et al. (2009) eliminated only 18% of aniline vapor using the same method.

Nonetheless, this predicting modeling was not without limitations. Indeed, it showed that the contact time had an important effect on adsorption yield. Its satisfactory adsorption operation was limited to 98 min. Beyond this contact time, it showed a steady decrease of the adsorption rate called the desorption process.

In parallel, the concentration of the pollutant would show a sharp increase to reach 100 mg/L. This would be equal to 10 times the adsorbent mass. Hence, it could be inferred that the saturation range of the nano- $Al_2O_3$  solid would be reached after 98 min of operation.

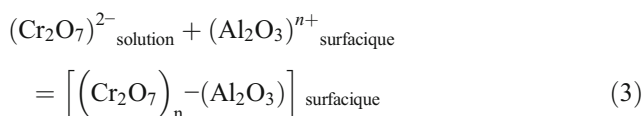
Moreover, as can be seen in Fig. 4, the adsorption yield decreases with the increase of temperature up to 318°K. This behavior seemed to be in contradiction with the commonly shared idea that the spontaneous reaction is always exothermic and increases with the increase of temperature and the wide agreement of scholars (Mor et al. 2007; Ayawei et al. 2015b; Crini et al. 2018; Sassi et al. 2020b) on the definition of the adsorption process as a spontaneous reaction. However, this observation will be discussed in more details in the “Thermodynamic studies” section below dealing with the thermodynamic study.

**Free adsorption process**

**Kinetic studies**

The study began with the equilibrium establishment of chromate (VI) adsorption onto alumina nanoparticles which was under the optimum conditions generated by the STATISTICA software.

The adsorption reaction was computed using the following equation at a chosen pH of 3.5:



In line with Ben-Ali et al. (2017), the adsorption quantity at the equilibrium was calculated according to the following equation

$$Q_e = \frac{(C_0 - C_e) \times V}{M} \quad (4)$$

where  $C_0$  and  $C_e$  are respectively the initial and the equilibrium concentration of Cr (VI) in solution (mg/L),  $Q_e$  is the equilibrium Cr (VI) ion concentration,  $M$  is the mass of the nanoparticles (0.01g), and  $V$  is the solution volume. Moreover, temperature and pH media were fixed at 318°K and 3.5, respectively.

Figure 5 shows the evolution of the adsorption yield of Cr (VI) on nano- $\text{Al}_2\text{O}_3$  function of contact time  $t_c$ .

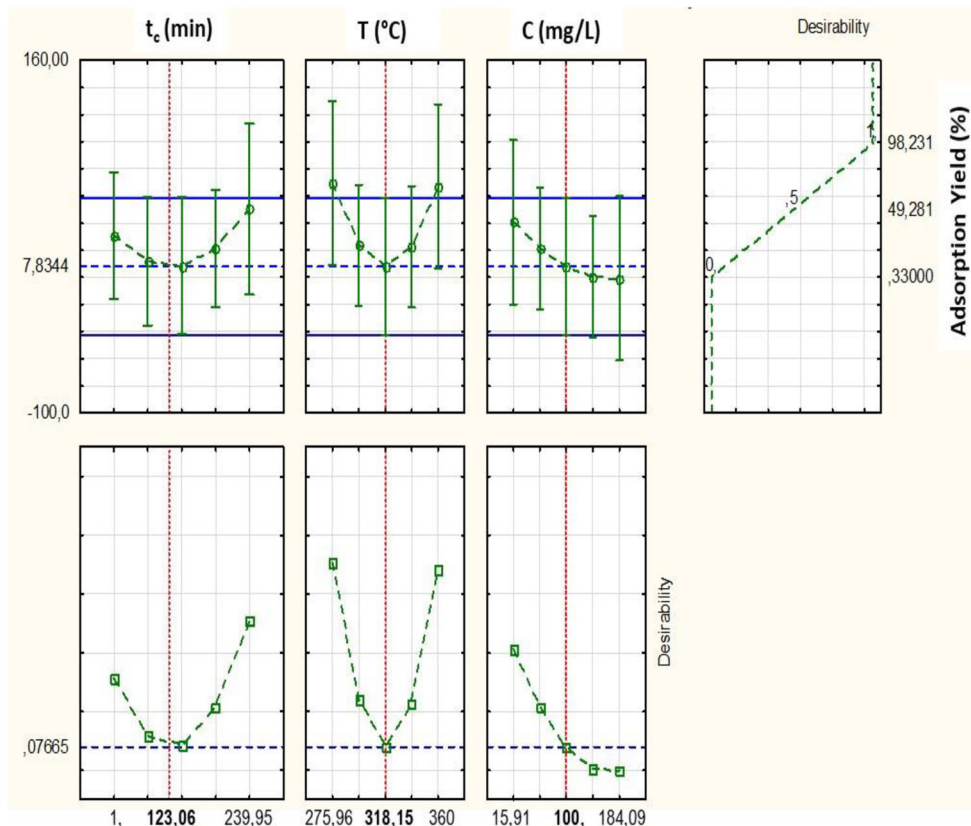
Figure 5 shows that the adsorption yield rose sharply for 60 min. Then, it started to curve slowly to reach its maximum yield of 87% after a contact time of 125 min. After that, it stabilized along a plateau during 250 min.

The adsorption rate was calculated graphically as the slope between points A and B

$$V_{\text{rate}} = \frac{Y_{(B)} - Y_{(A)}}{t_{c(B)} - t_{c(A)}} = \frac{90.86 - 52.48}{125.52 - 32.70} = 0.413\%/\text{min} \quad (5)$$

- This average adsorption rate was relatively higher than adsorption rates. The removal of thallium, Born, hexavalent chromium, chromate, and dies was reported by Zhang et al. (2008), Seki et al. (2006), Pakade et al.

**Fig. 4** Graphic presentation of the optimum conditions of the chromate adsorption on nano- $\text{Al}_2\text{O}_3$



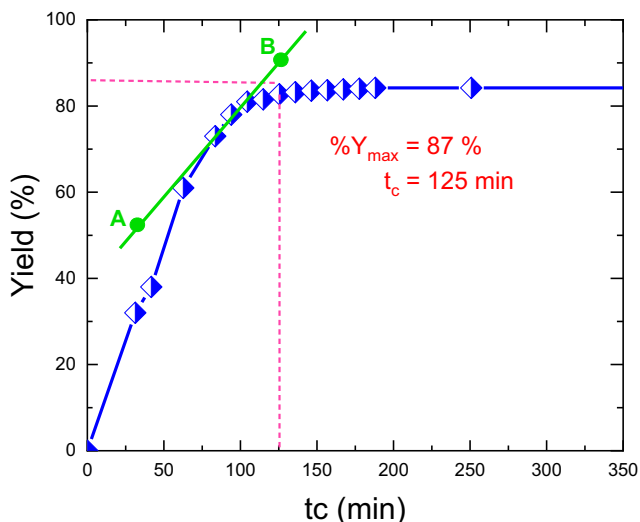


**Fig. 5** Adsorption yield of Cr (VI) on nano- $\text{Al}_2\text{O}_3$  function of contact time (pH 3.5 and  $T = 318^\circ\text{K}$ )

(2019), Guzel et al. (2016), and Marzouk Trifi et al. 2019, respectively. Yet, this rate was much higher than when the adsorbent was extracted from biocompounds (17, 34) where the adsorption rate was only 0.3–0.8 %/min. However, despite the clear improvement of this rate, it was still lower than that achieved by activated alumina reported by Marzouk Trifi et al. (2019).

Pseudo-first order (PFO), pseudo-second order (PSO), intra-particle diffusion (IPD), and Elovich models were employed to study the adsorption kinetic of chrome (VI) on  $\text{Al}_2\text{O}_3$  nanoparticles. All information about those kinetics models and their curves are detailed in a [supplementary data file](#).

Table 3 summarizes all the results obtained.

As can be seen in Table 3, the process of chrome adsorption on nanoparticles  $\text{Al}_2\text{O}_3$  would not be a chemisorption because  $R^2$  was equal to 0.85218 for the Elovich model. In addition, the regression coefficient of the PFO kinetic was high ( $R^2=0.9928$ ). Therefore, it can be concluded that this process followed the PFO model which would imply that the reaction rate depended only on the chromate concentration. This finding was in total agreement with Saxena et al. (2009), Morozova et al. (2020), and Nie et al. (2020). Moreover, it seems that this finding was

**Table 3** Pseudo-First-Order (PFO), Pseudo-Second-Order (PSO), Intra-Particle Diffusion (IPD) and Elovich constants and model correlation coefficients

Pseudo-first order (PFO)			Pseudo-second order (PSO)		
$k_1$	$Q_e$	$R^2$	$k_2$	$Q_e$	$R^2$
-0.0251	38.7444	0.9928	0.0005	7.1855	0.7442
Intra-particle diffusion (IPD)			Elovich		
$k_3$	$R^2$	$\alpha$	$B$	$R^2$	
0.18898	0.8762	0.0685	0.9201	0.85218	

related to the nature of the adsorbent/adsorbate. Indeed, like this study, all the cited works treated mineral adsorbent/adsorbate. Hence, in line with all these scholars, it can be concluded that the adsorption was a physisorption with the formation of one layer. The study of the isotherms, below, would either confirm or reject this proposition.

**Isotherm studies**

The isotherm study was conducted to understand the adsorption mechanism of Cr (VI) on alumina nanoparticles and their surface affinity under the optimum conditions, i.e.,  $T = 318^\circ\text{K}$ , pH = 3.5, and  $t_c = 123$  min.

Figure 6 shows the graphic presentation of the adsorption quantity of Cr (VI) on  $\text{Al}_2\text{O}_3$  nanoparticles in function of chromate concentration at equilibrium  $C_e$ . The adsorption isotherm was determined using Eq. 4. As can be seen in Fig. 6, the standard adsorption isotherm reached a maximum adsorption of Cr (VI) equal to 221 mg/g for a  $C_e$  equal to or higher than 216 mg/L.

This result would imply that the nanoparticles of raw alumina were saturated faster than activated alumina which had a  $Q_{e(\text{max})}$  equal to 350 mg/g. This finding corroborated with results reported by Yadav and Bhattacharyya (2019), Cai et al. (2009), and Marzouk-Trifi et al. (2019). The shape of the graph in Fig. 6 would match that of a typical adsorption isotherm into micropores as was described by Králik (2014).

In order to understand the adsorption mechanism, some isotherms were chosen to assess their corroboration with the experimental data reported by Ayawei et al. (2015a, 2015b, 2017): Langmuir, Freundlich, Temkin, and Dubinin-Radushkevich. Firstly, the Langmuir isotherm was primarily designed to quantify and contrast the adsorptive capacity of the adsorbents. The goal of this model was to balance the

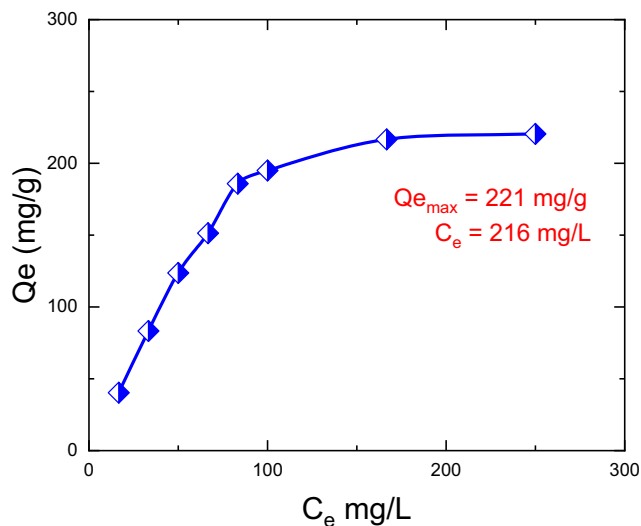


**Fig. 6** Adsorption isotherm of Cr (VI) on nano- $\text{Al}_2\text{O}_3$  at  $t_c = 123$  min, pH 3.5, and  $T = 318^\circ\text{K}$

relative rates of the adsorption/desorption process known as dynamic equilibrium as was shown by Ayawei et al. (2015a, 2015b, 2017).

In line with Králik (2014) and Crini et al. (2018), the linear form of the Langmuir equation can be written as follows:

$$\frac{C_e}{Q_e} = \frac{1}{Q_m k_L} + \frac{C_e}{Q_m} \tag{6}$$

where,

- $C_e$  is the equilibrium Cr (VI) concentration (mg/L);
- $Q_e$  and  $Q_m$  are the equilibrium and the theoretical maximum adsorption capacities, respectively (mg/g);
- $k_L$  is the Langmuir constant (L/mg).

Figure 7A illustrates the plot of  $C_e/Q_e$  in function of  $C_e$ . Table 4 summarizes the Langmuir parameters. Figure 7A clearly shows that the experimental data fitted the regression coefficient of about  $R^2 = 0.9700$ . This behavior would suggest a monolayer adsorption of chromate (VI) on  $Al_2O_3$

**Table 4** Langmuir, Freundlich, Temkin, and Dubinin-Radushkevich constants and model correlation coefficients

Langmuir			Freundlich		
$k_L$	$Q_m$	$R^2$	$k_F$	$N$	$R^2$
0.0171	90.9091	0.9700	13.2199	1.3437	0.8055
Temkin			Dubinin-Radushkevich		
$k_T$	$A$	$R^2$	$Q_s$	$B$	$R^2$
0.180	73.3339	0.9373	3.5434	0.0011	0.9733

nanoparticles known as one dimension (1D) adsorption process as named by Sadeghi et al. (2020) and Hou et al. (2020). Even the scattered points around the median line, especially at  $C_e \leq 50$  mg/L and at  $C_e \geq 100$  mg/L did not diverge from the median line in a significant way.

As is clearly seen in Table 4, the Langmuir parameters had a maximum monolayer  $Q_m$  equal to 90.91 mg/g at the optimum temperature. The Langmuir isotherm also defined a dimensionless separation parameter  $R_L$  in function of the following Eq. 7:

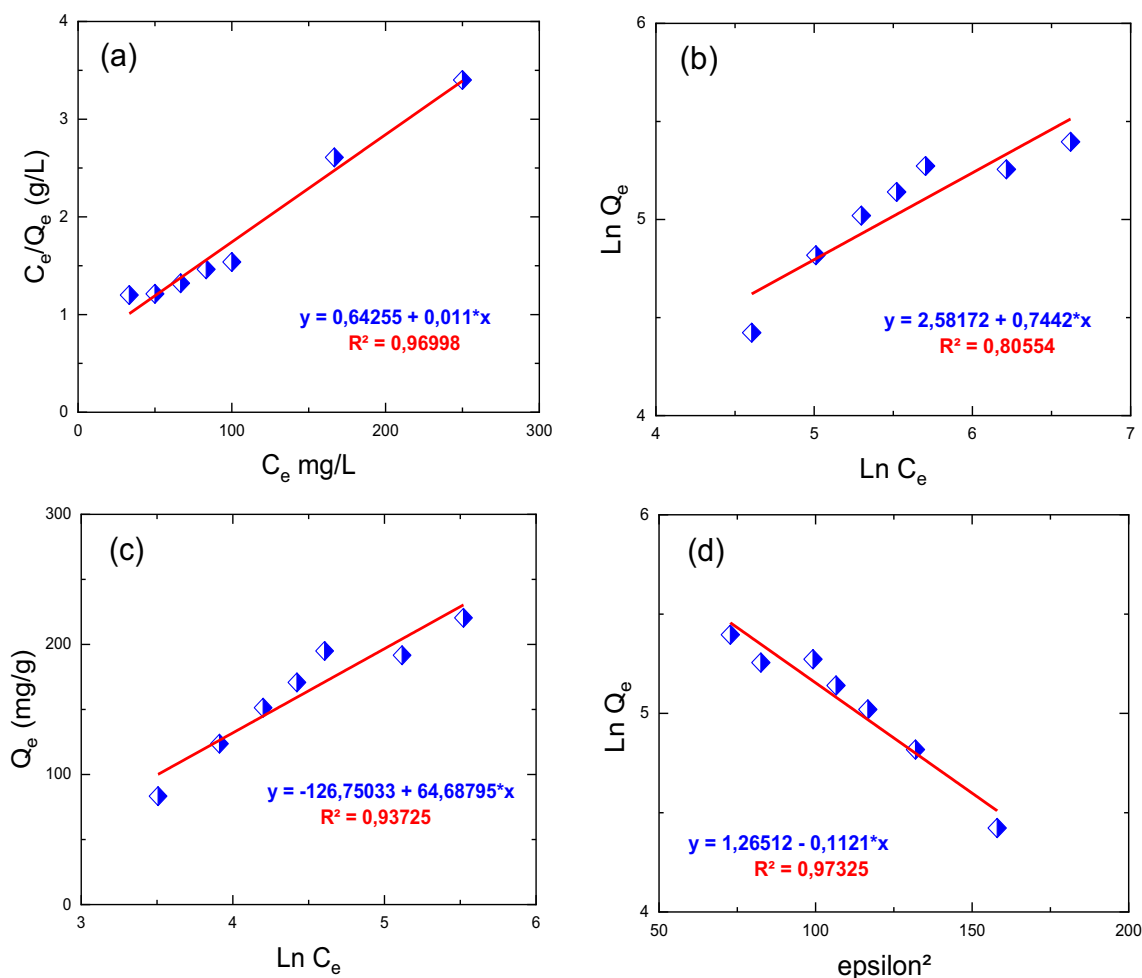


**Fig. 7** Linear isotherms plots. (A) Langmuir, (B) Freundlich, (C) Temkin, and (D) Dubinin-Radushkevich isotherms of Cr(VI) on  $Al_2O_3$  nanoparticles ( $T = 318^\circ K$ ,  $t_c=123$  min,  $pH = 3.5$ )



$$R_L = \frac{1}{1 + k_L \times C_0} \tag{7}$$

where,

$C_0$  is the initial concentration of the model (mg/L);  
 $k_L$  is the Langmuir constant (L/mg).

The parameter  $R_L$  was differently interpreted by Králik (2014) and Ayawei et al. (2015a, 2015b, 2017). However, the main conclusions were as follows:

- $R_L > 1$  The adsorption is unfavorable.
- $R_L = 1$  The adsorption is linear.
- $R_L < 1$  The adsorption is favorable.
- $R_L = 0$  The adsorption is irreversible.

In the studied process,  $R_L$  ranged  $\in [0.66; 0.19]$  when the  $C_0$  ranged  $\in [30; 250]$ .

This result suggests that the adsorption of Cr (VI) on alumina nanoparticles was a favorable process and it happened as a monolayer adsorption without interaction between the chromate ions. To evaluate the multilayer adsorption, other models were tested.

Secondly, the Freundlich isotherm was also studied. This isotherm was applicable to adsorption processes on heterogeneous surfaces as we reported by Ayawei et al. (2015a, 2015b, 2017).

Therefore, the model could offer a good description of the surface heterogeneity, the distribution of active sites, and even their surface energies as was recommended by Ayawei et al. (2015a, 2015b, 2017). For the Freundlich isotherm, the Ln-Ln version was used in the following Eq. 8:

$$\text{Ln } Q_e = \text{Ln } k_F + \frac{1}{n} \text{Ln } C_e \tag{8}$$

where,

- $k_F$  is the Freundlich constant (L/mg).
- 1/  $n$  this parameter has many interpretations; adsorption intensity (44), coefficient of energy’s distribution (48), and heterogeneity of the adsorbate sites (45). Generally, when the parameter  $n$  is positive, it indicates the number of the multilayer’s adsorption onto the adsorbent (Ho 2000; Romero-González et al. 2005; Srihari and Das 2008; Saxena et al. 2009).

Figure 7B illustrates the plot of Ln ( $Q_e$ ) in function of Ln ( $C_e$ ). The Freundlich modelization differed from the Langmuir fitting since it was non-linear and showed points scattered around the median line. Table 4 summarizes the Freundlich parameters

The low regression coefficient  $R^2$  was 0.8055, which would imply that the experimental data did not fit the model. This result would imply that the adsorption of chromate (VI)

on nano- $\text{Al}_2\text{O}_3$  did not occur on a heterogeneous surface. This observation would be a soundproof of the purity and homogeneity of the synthesized alumina nanoparticles. In addition, as was theorized by Freundlich (Freundlich 1928), since the adsorption coefficient intensity  $n$  was  $< 2$ , it confirmed a monolayer adsorption. In addition, since it was also  $> 1$ , it indicated a favorable adsorption process. This finding corroborates with that reported about the Langmuir isotherm.

Because adsorption of Cr (VI) on nano- $\text{Al}_2\text{O}_3$  was found to fit the Langmuir model but did not fit the Freundlich one, models combining Langmuir and Freundlich such as Langmuir-Freundlich, Redlich-Peterson, Sips, Toth, and Koble-Carrigan isotherms were excluded in this study.

Thirdly, the Temkin isotherm model which considered the effects of indirect adsorbate/adsorbate interactions during the adsorption process was applied. However, as was indicated by Shahbeig et al. (2013) and Araújo et al. (2018), it was valid only for an intermediate range of ions concentrations; i.e., ignoring very low and very high concentration values. The linear form of the Temkin isotherm model is shown in Eq. 9 as reported by Ayawei et al. (2015a, 2015b, 2017):

$$Q_e = A \text{Ln } k_T + A \text{Ln } C_e \tag{9}$$

where,

- $A = (RT)/b$   $R$  is the gas constant ( $8.314 \text{ J mol}^{-1} \text{ K}^{-1}$ ),  $T$  is the absolute temperature at  $318^\circ\text{K}$ , and  $b$  is the Temkin constant related to the heat of adsorption (J/mol).
- $k_T$  is the Temkin binding constant (L/g).

Figure 7C illustrates the plot of  $Q_e$  in function of Ln ( $C_e$ ). Despite the spread of recorded experimental points, the regression coefficient was 0.9372. Consequently, the adsorption process fitted the Temkin model than the Freundlich one. Table 4 summarizes the Temkin model parameters.

The graphically calculated parameters of this model, namely  $k_T = 0.180$  (L/g) and  $A = (RT/b) = 73.334$  would imply that the Temkin constant  $b$  was equal to  $36.0522$  J/mol. Obviously, this value was  $< 8000$  J/mol, which would imply that the mechanism involved was a physical adsorption. Araújo et al. (2018) explained the weak adsorbate/adsorbent adhesion by Van Der Waals’s interactions because it was associated with relatively low adsorption energies. In addition, these scholars related the Temkin constant  $b$  to the sorption heat in relationship  $b = f(\Delta H)$ . Therefore, if  $b$  had a positive value, the adsorption reaction would be endothermic. However, if  $b$  had a negative value, the sorption would be exothermic (Araújo et al. 2018). In this work, the  $b$  coefficient was positively charged; consequently, the adsorption reaction would be endothermic. Hence,  $\Delta H$  would be positive. This result will be discussed in more detail in the “Thermodynamic studies” section below dealing with the thermodynamic study.

Finally, the Dubinin-Radushkevich isothermal adsorption parameters along with their determination coefficient  $R^2$  are presented in Table 4. This model was applied in order to investigate the mechanism nature of the adsorption process involved in the heterogenous potential surface. The linear formula was expressed by Kozłowski and Pallardy (2002) and Roundhill and Koch (2002) in the following Eq. 10.

$$\ln Q_e = \ln Q_s - B \varepsilon^2 \quad (10)$$

where,

$Q_s$  is the theoretical saturation monolayer capacity of the nano- $\text{Al}_2\text{O}_3$  (mol/g);

$B$  is medium free energy ( $\text{mol}^2 \text{K J}^2$ );

$\varepsilon$  is Polanyi potential expressed as  $\varepsilon = RT \ln \left( 1 + \frac{1}{C_e} \right)$

when  $R$  is the gas constant ( $8.314 \text{ J mol}^{-1} \text{ K}^{-1}$ ), and  $T$  is the absolute temperature ( $^\circ\text{K}$ ).

Figure 7D illustrates the plot of  $\ln Q_e$  in function of  $\varepsilon^2$ . The recorded regression coefficient was  $R^2=0.9733$ . This result would imply that the Dubinin-Radushkevich model could fit well our experimental data. A parameter  $E$  proposed by Kozłowski and Pallardy (2002) could help to distinguish the adsorption type. The formula proposed by Kozłowski and Pallardy (2002) is presented in the following Eq. 11:

$$E = \frac{1}{\sqrt{2B}} \quad (11)$$

where if:

- ✓  $E \in [1-7] \text{ kJ mol}^{-1}$  is a physisorption as was determined by Kozłowski and Pallardy (2002);
- ✓  $E \in [8-15] \text{ kJ mol}^{-1}$ , is ion exchange as was determined by Yüksel and Orhan (2019);
- ✓  $E > 16 \text{ kJ mol}^{-1}$ , is a chemisorption as was determined by Yüksel and Orhan (2019);

In this study, the  $E$  value was  $2.112 \text{ kJ mol}^{-1}$  confirming a physical adsorption or physisorption as proposed in the “Kinetic studies” section above dealing with the kinetic study (Elovich model). This result supports previous findings by Mor et al. (2007, 2018) despite the weak correlation of  $R^2=0.8937$ . To confirm this result, thermodynamic parameters had to be studied.

### Thermodynamic studies

There are many methods to find numeric values of the thermodynamic parameters as free energy of Gibbs ( $\Delta G^\circ$ ), enthalpy ( $\Delta H^\circ$ ) et entropy ( $\Delta S^\circ$ ).

In this study, the equation proposed by Romero-Gonzalez et al. (2005) and Belaid and Kacha (2011) was used

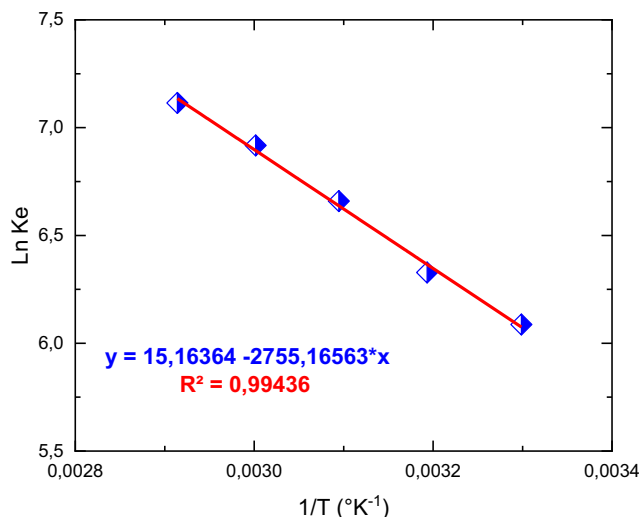


**Fig. 8** Determination of the thermodynamic parameters of Cr (VI) adsorption on  $\text{Al}_2\text{O}_3$  nanoparticles with  $t_e = 123 \text{ min}$  and  $\text{pH} = 3.5$

$$K_e = \frac{Q_e}{C_e} \quad (12)$$

$$\Delta G^\circ = -RT \ln K_e \quad (13)$$

$$\ln K_e = \frac{\Delta S^\circ}{R} - \frac{\Delta H^\circ}{R} \times \frac{1}{T} \quad (14)$$

where  $K_e$  is the equilibrium constant,  $Q_e$  is the amount of solute (mol) adsorbed on the adsorbent cubic decimeter of the solution at equilibrium,  $C_e$  is the equilibrium concentration (mol/L) of the solute in solution,  $T$  is the temperature in  $^\circ\text{K}$ , and  $R$  is the gas constant.

Figure 8 shows  $\Delta H^\circ$  and  $\Delta S^\circ$  values obtained from the slope and intercept of Van'Hoff plots of  $\ln K_e$  in function of  $1/T$ . Table 5 shows the calculated values of the thermodynamic parameters.

The negative values of the free enthalpy  $\Delta G^\circ$  obtained at different temperatures would confirm the thermodynamic spontaneity of the Cr (VI) adsorption reaction on  $\text{Al}_2\text{O}_3$  nanoparticles.

Moreover, the enthalpy value  $\Delta H^\circ$  was approximately  $23 \text{ kJ/mol}$ , i.e., much lesser than  $80 \text{ kJ/mol}$ .

**Table 5** Thermodynamic parameters of the chromate adsorption process on  $\text{Al}_2\text{O}_3$  nanoparticles

$T$ ( $^\circ\text{K}$ )	$\Delta G^\circ$ (kJ/mol)	$\Delta H^\circ$ (kJ/mol)	$\Delta S^\circ$ (J/mol $^\circ\text{K}$ )
303.15	-15.34104	22.9064	126.0705
313.15	-16.47497		
323.15	-17.89132		
333.15	-19.16072		
343.15	-20.29808		

This result would confirm the existence of a physisorption process since physical adsorption implies an interaction between adsorbent/adsorbate. In addition, all  $\Delta G^\circ$  values were negative while both  $\Delta H^\circ$  and  $\Delta S^\circ$  values were positive. Srihari and Das (2008) and Araújo et al. (2018) theorized that for an entropy to occur, the increase must overcome the handicap of an endothermic process. Therefore,  $T\Delta S$  must be greater than  $\Delta H$ . Since the effect of the temperature is to boost the effect of a positive  $\Delta S$ , then the process will be spontaneous at temperatures above the quotient  $T = \Delta H / \Delta S$ . In general, this quotient was found to be  $T > 181^\circ\text{K}$ . In this study,  $T$  was equal to  $318^\circ\text{K}$ . Consequently, it can be concluded that the adsorption process occurring would be an endothermic and spontaneous physisorption. This would perfectly corroborate with the kinetic isotherm interpretations.

So far, this study proved that the adsorption was not only possible, but it occurred spontaneously. Nevertheless, this process could yield only a maximum of 87% which could be preferably improved to become more satisfactory. Besides, the  $\text{Al}_2\text{O}_3$  particles could reach their maximum yield only after 98 min of contact time. Therefore, this study attempted to test an applied current density to the reactor to enhance the yield and decrease the contact time before reaching the maximum yield.

### Electrosorption

All electrochemical tests were conducted at the optimum conditions generated by the software STATISTICA ( $t_c = 123$  min,  $T = 318^\circ\text{K}$ , and  $C_0 = 100$  mg/L). On the other hand, in order to determine the exact applied current value required to achieve a total electrosorption of the Cr (VI) ions on  $\text{Al}_2\text{O}_3$  nanoparticles, a cyclic voltammetry of the bath containing only chromate ions was adopted.

The voltammetry test was two cyclic scans from open circuit potential  $E_0$  to a cathodic potential  $E_1$  ( $-1.5$  V/AgCl) after that returning to an anodic potential  $E_2$  ( $+1.5$  V/AgCl) using a scanning rate of  $0.025$  V/min. Figure 9 shows the obtained cyclic voltammetry of the reactor content.

The cyclic voltammetry shows that chromate ions needed a cathodic current of about  $-20$  mA/cm<sup>2</sup> to be reduced onto a solid surface. Therefore, the electrosorption bath was conducted using the chronopotentiometry method in the same sample used for the free adsorption process with  $t_c = 123$  min,  $T = 318^\circ\text{K}$ ,  $\text{pH} = 3.5$ , and an amount of alumina nanoparticles at  $100$  mg/L. In addition, the applied current density was  $-20$  mA/cm<sup>2</sup> at optimum conditions. The pH of the solution was controlled by a titrimeter-fisher probe and remains constant during the electrosorption process.

Figure 10 shows the obtained chronopotentiometry plots.

Figure 10 shows that the potential of the electrolyte increased from  $-8$  to  $-5$  V/AgCl for the first 5 min. This behavior would indicate both the decrease of the ionic force of the

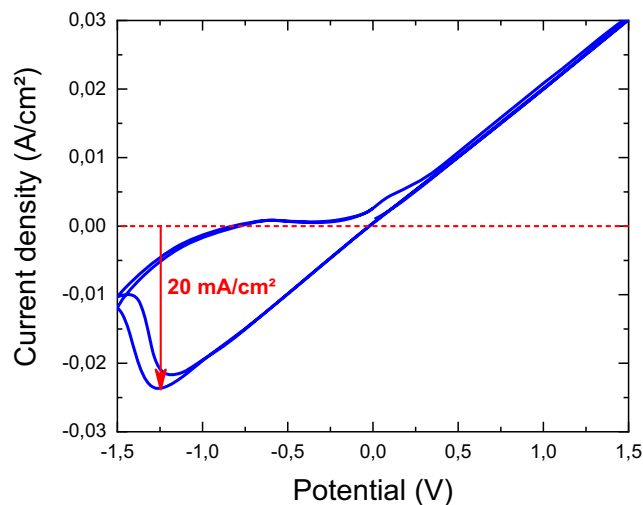


Fig. 9 Cyclic voltammetry of the reactor during electrosorption of Cr (VI) on  $\text{Al}_2\text{O}_3$  nanoparticles at  $\text{pH} = 3.5$  and  $T = 318^\circ\text{K}$

bath and the electric conductivity of the electrolyte. In addition, the potential of the system stabilized at  $-3.5$  V which would imply the dynamic equilibrium of the electrosorption process. The presence of small potential fluctuations beyond 20 min might be an indication of local perturbations of zeta surface potential of the material. The presence of small

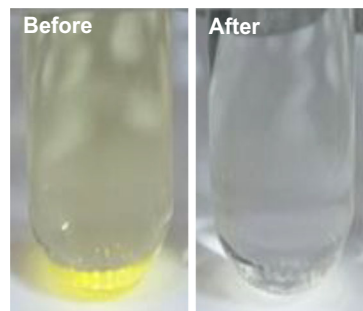
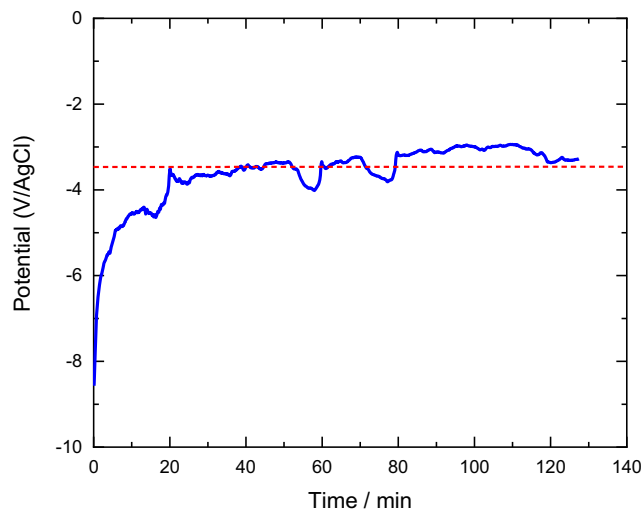


Fig. 10 Chronopotentiometry plot recorded for free-chromates bath and during electrosorption of Cr (VI) on  $\text{Al}_2\text{O}_3$  nanoparticles at  $\text{pH} = 3.5$  and  $T = 318^\circ\text{K}$  and solution pictures before and after electrosorption

potential fluctuations beyond 20 min might be an indication of local perturbations of zêta surface potential of the material. Moreover, UV analysis shows that the adsorption yield recorded was 98% and was reflected by the discoloration of the chromate solution.

More importantly, the full discoloration occurred after only 20 to 25 min after the beginning of the electrosorption process. This time was much shorter than the 123 min needed in the free adsorption process for the  $\text{Al}_2\text{O}_3$  nanoparticles to reach their maximum yield.

However, for a better comparison of the two processes, it would be very useful to conduct a study of the morphology of the  $\text{Al}_2\text{O}_3$  in the two processes.

### Comparison between free and electro-adsorption process

#### SEM and EDS studies

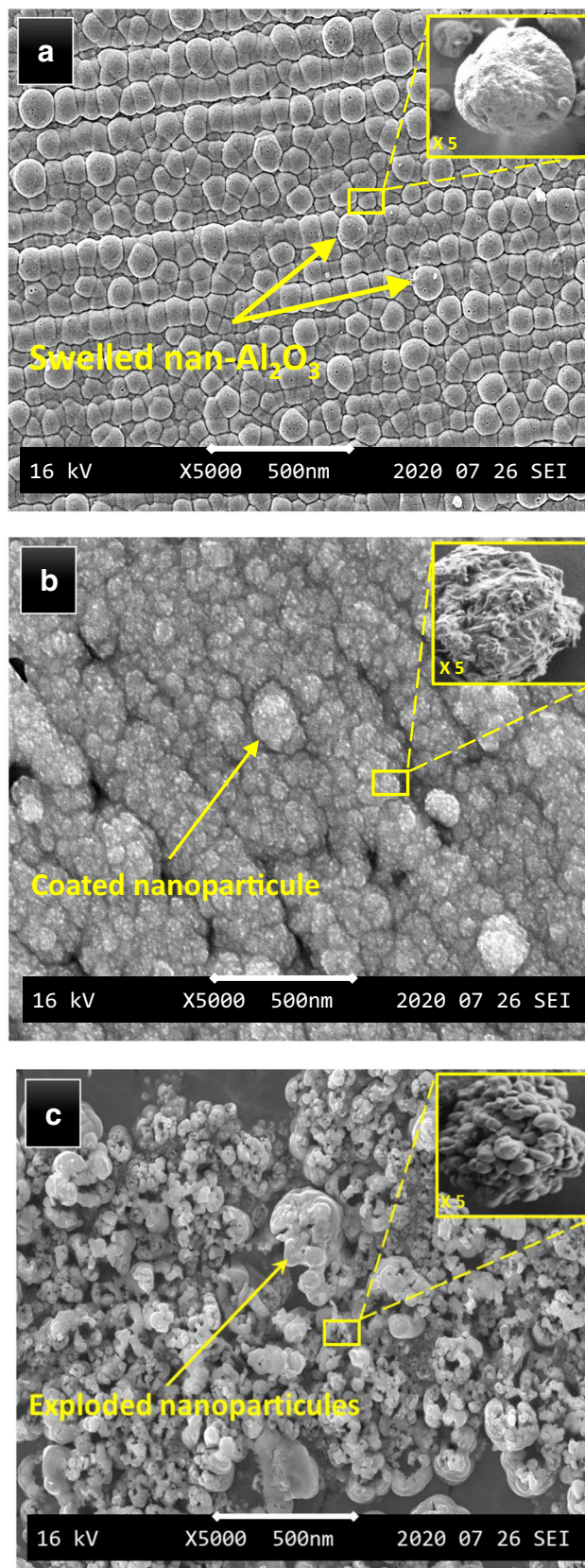
Figure 11 exhibits SEM spectra of  $\text{Al}_2\text{O}_3$  nanoparticles in their raw form after undergoing a washing/drying cycle, after free adsorption of Cr (VI) and after electro-adsorption of the same contaminant. All samples were obtained with the optimum conditions.

Fig. 11(A) shows the raw nanoparticles after undergoing the washing/drying cycle at pH 3.5 and  $T=318^\circ\text{K}$ . These  $\text{Al}_2\text{O}_3$  particles seem to have more than doubled their original size of 30 nm to reach 70 nm. Lamouri et al. (2017) and Marzouk Trifi et al. (2019) reported a similar observation and explained this phenomenon by the fact that there was a high readiness of the  $\alpha$ -alumina phase to adsorb water anions ( $\text{OH}^-$ ) at acidic pH.

The SEM micrographs of the nanomaterial after the free adsorption process of Cr (VI) are shown in Fig. 11B. The roughness of the nanoparticle surface was clear and some light points were easy to locate at the surface. The roughness and the light points could be identified as the adsorbed chromate anions. If the explanation was limited to the physisorption, as was strongly argued in the isothermal and thermodynamical studies, the functional nanoparticles would be swelled due to the massive adsorption of chromate anions onto their surface. Moreover, as was rightly explained by Nordfors et al. (1992), when the adsorbate is tied to the surface by dispersion forces only, i.e., when short-range bonding effects are small, all multilayer adsorptions are weak and thus neglected. Therefore, it would be very coherent to conclude that the experimental data would not fit the Freundlich model studied in the ‘‘Isotherm studies’’ section, which predicted the existence of a multilayer adsorption.

Fig. 11C displays an SEM graph of  $\text{Al}_2\text{O}_3$  nanoparticles after electroadsorption of Cr (VI).

The nanoparticles seem to have exploded in a helix form. The magnification of one specific sample shows a mass of



**Fig. 11** SEM micrographs of (A) raw  $\text{Al}_2\text{O}_3$  nanoparticles, (B)  $\text{Al}_2\text{O}_3$  nanoparticles after free adsorption of Cr (VI), and (C)  $\text{Al}_2\text{O}_3$  nanoparticles after electroadsorption of Cr (VI). All samples were obtained at pH = 3.5 and  $T = 318^\circ\text{K}$

nanoparticles bonded to each other. Arukula et al. (2019) reported a similar phenomenon and called it “coagulation under electric field or electrocoagulation.” This can be considered a completely different adsorption process.

Fig. 12 shows the energy-dispersive x-ray spectra and map of Cr (VI) and nano- $\text{Al}_2\text{O}_3$ .

The elemental composition investigated by the EDS technique presented a regular dispersion of the chrome anions on  $\text{Al}_2\text{O}_3$  nanoparticles. This observation corroborates with the finding on the homogeneity of the nanoparticles surface reported in the “Isotherm studies” section above treating the isotherm analysis. In addition, Fig 12A which exhibits

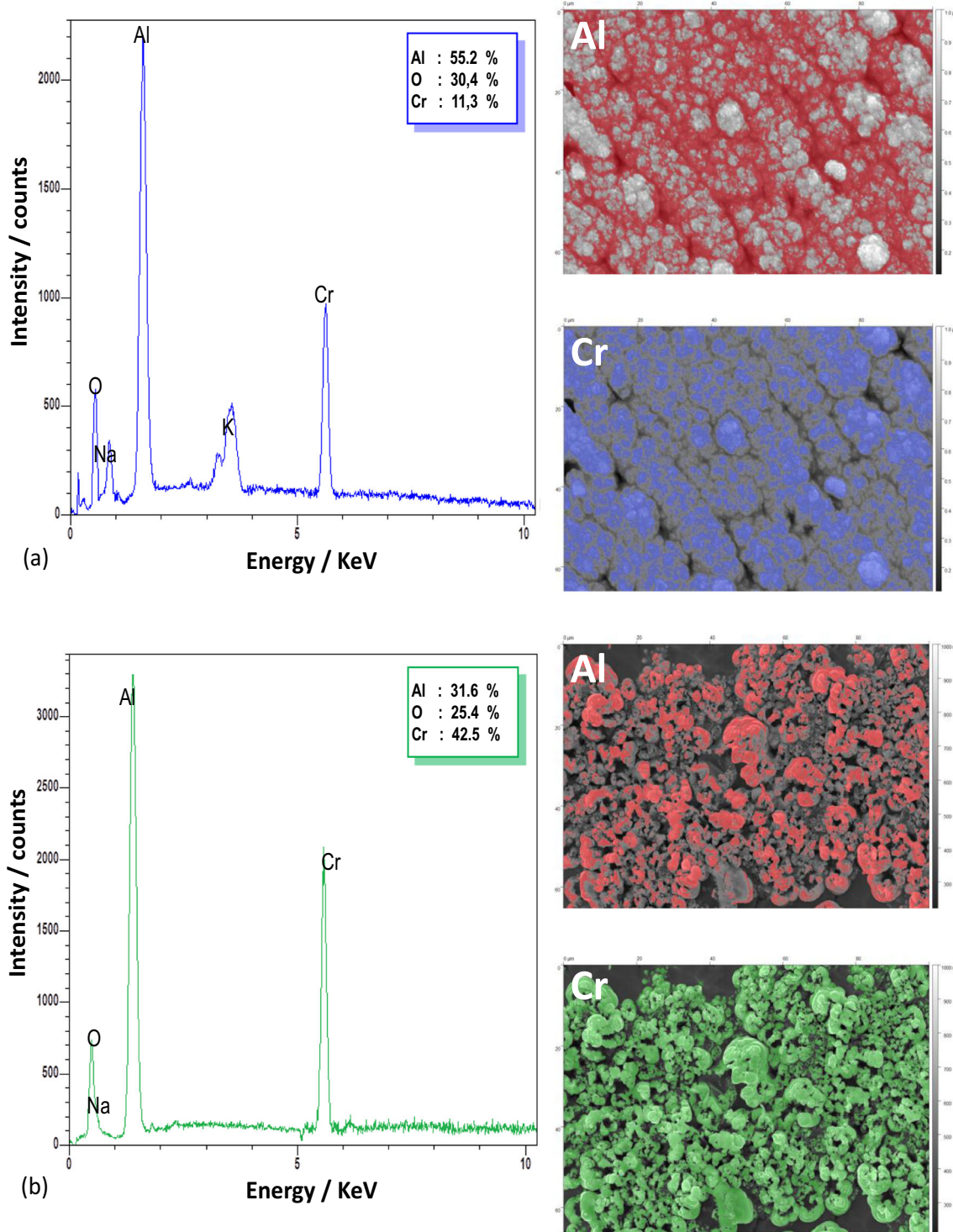


Fig. 12. Energy-dispersive x-ray spectra and map of Cr (VI) and nano- $\text{Al}_2\text{O}_3$  after (A) free adsorption and (B) electrosorption. All samples were obtained at  $\text{pH} = 3.5$  and  $T = 318^\circ\text{K}$

Al<sub>2</sub>O<sub>3</sub> nanoparticles after free adsorption of Cr (VI) shows that Cr (VI) was omnipresent on nanoparticle surfaces. Nevertheless, the amount of Cr (VI) in EDS spectra was only about 11% which would present less than one-third of the Al content. This discrepancy between the spread of Al and its real rate was reported by Karoui et al. (2020) and Marzouk Trifi et al. (2019) who agreed that it could be explained by the fact that the adsorption capacity of alumina stabilized at 100 min, but the adsorption process continued slowly.

Finally, Fig 12B which exhibits Al<sub>2</sub>O<sub>3</sub> nanoparticles after electrosorption process adsorption of Cr (VI) shows the presence of chromium onto exploded nanoparticles in the form of irregular islands on the on-material edge. Hence, it can be inferred that the chromium loaded onto Al<sub>2</sub>O<sub>3</sub> nanoparticles contributed to the irregularity of their surface. This would plausibly explain their unusual helix structure. Finally, this would imply that the crystallinity of the alumina could be controlled.

### UV-Vis and XRD analysis

Figure 13 presents the UV spectra of Cr (VI) and XRD spectra of the nanoparticles before and after both free adsorption and electrosorption processes. A pure chrome solution and raw nano-Al<sub>2</sub>O<sub>3</sub> particles were used for comparison purposes.

Figure 13 shows the UV-Vis spectra and the XRD spectra of nano-Al<sub>2</sub>O<sub>3</sub> before and after free adsorption and after electrosorption. In Fig. 13A, the UV-Vis spectra exhibited a clear decrease of chromate ion peak for both free and electro-adsorption reflecting a drop of the absorbance. Moreover, after electrosorption, the sample absorbance was less than 0.1 u.a which would explain the recorded highest yield of 99%. In parallel, the existence of a unique absorption peak in these UV spectra for all the samples would strongly prove the absence of decomposition reactions.

Fig. 13B exhibits the XRD spectra of nano-Al<sub>2</sub>O<sub>3</sub> before adsorption, after free adsorption, and after electrosorption. It can be easily observed that in the latter process, the peaks decreased noticeably signaling that the nano-Al<sub>2</sub>O<sub>3</sub> lost some of their crystallinity after the application of a current density. Additionally, the broad peak of about 43° would be very likely a signal of the material explosion. This last observation induced a divergence of opinions among researchers about the sustainability of the alpha phase of nanoparticles and especially alumina oxide. Indeed, whereas researchers like Díaz-Sánchez et al. (2019), Crini et al. (2018, 2019), and Wakabayashi et al. (2020) argued that the alpha phase needed specific thermodynamical conditions to decompose or rearrange; other scholars such a Kumari et al. (2020) contended that the alpha phase is naturally instable. This work argues that a logical explanation of these explosions would be that the nanoparticles were electrically forced to adsorb massive chromate anions which destabilized its crystalline structure by increasing the atomic disorder and therefore its crystal entropy.

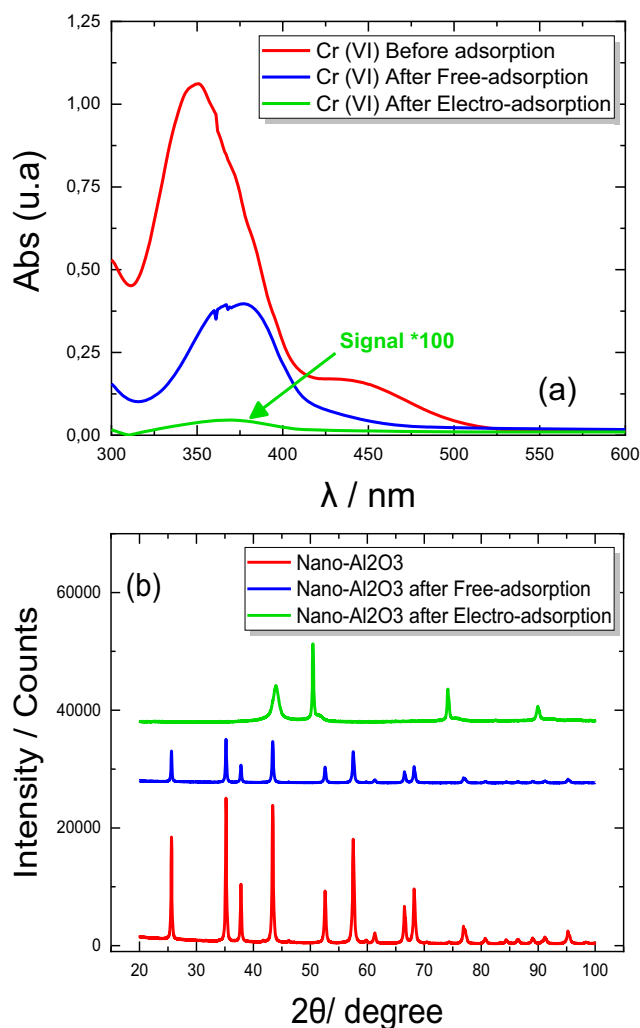


**Fig. 13** (A) UV-Vis spectra of Cr (VI) solutions and (B) XRD spectra of nano-Al<sub>2</sub>O<sub>3</sub> before adsorption after free adsorption and after electrosorption. All samples were obtained at pH = 3.5 and  $T = 318^{\circ}\text{K}$ .

Kumari et al. (2019, 2020), Kumar et al. (2011), and Guan et al. (2009) agreed that all these observations would serve to prove the helix structure of the nanoparticles. Moreover, the shift of the XRD peaks would indicate the change in the preferred plan and thus confirm the incorporation of adsorbate not only into the adsorbent but also over and around it. The absence of chromate peaks would be due to the alumina broad peaks which would hide them.

### Free and electro-adsorption mechanisms

Figure 14 presents a graphic presentation of the mechanism occurring during the adsorption process.

As can be seen in Fig. 14A, the free-adsorption process would occur spontaneously, one-layer adsorption and as a physisorption. Indeed, the nanoparticles Al<sub>2</sub>O<sub>3</sub> positively charged in acidic media of pH = 3.5. Accordingly, the electrostatic attraction might be the reason for the chromate

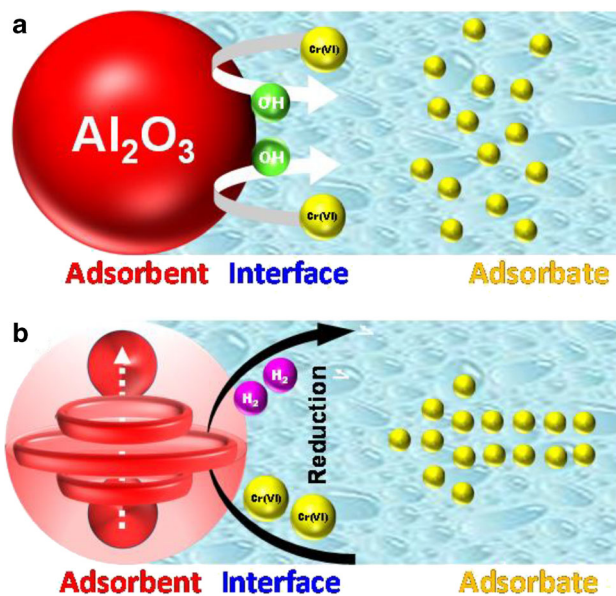


**Fig. 14** Graphic presentation of the mechanism occurring during the adsorption process. (A) During the free adsorption. (B) During the electro-sorption. All samples were obtained at pH = 3.5 and  $T = 318^{\circ}\text{K}$

adsorption by ion exchange with anions (probably water hydroxyls).

However, as can be seen in Fig. 14B, the applied current density used in the electro-sorption process would create an electric field between anode/cathode electrodes which would trap the nanoparticles. In this adsorbent/adsorbate concentrated space, the chromate ions would be reduced on the alumina surface. This reduction would continue until changing the areal zeta potential of the adsorbent. The atomic disorder would increase with entropy increase. Crystals would become unstable, and the nanoparticles would explode forming the famous helix structure.

## Conclusion

This study attempted to design and assess the performance of a satisfactory and environment-friendly adsorbent for dechromation purposes.

The main results of this study were of two categories. Firstly, in terms of comparison between electro-sorption and free adsorption, the former was rather more efficient since it could remove 99% of Cr (VI) while free adsorption removed only 87%. In addition, the electro-sorption reached its maximum capacity in only 20 to 25 min while free adsorption needed no less than 123 min to do the same. Secondly, in terms of attempts to explain the mechanisms occurring in this phenomenon, this study revealed that the alumina nanoparticles would lose their crystallinity after the application of  $20 \text{ mA/cm}^2$ . Then, whereas the free-adsorption would occur as an electrostatic interaction between adsorbent/adsorbate and exchange ions-ions reaction,

the electro-sorption would occur in the double-layer interface of the nano- $\text{Al}_2\text{O}_3$  and would lead to nanoparticle explosion. Finally, EDS analysis showed that after electro-sorption, the amount of Cr (VI) absorbed on nano- $\text{Al}_2\text{O}_3$  was 42.5 % while after free adsorption, it was only 11.3%.

In conclusion, this study revealed that the electro-sorption was faster and slightly more efficient than free adsorption in the treatment of wastewaters contaminated with Cr (VI).

**Supplementary Information** The online version contains supplementary material available at <https://doi.org/10.1007/s11356-021-12612-7>.

**Acknowledgements** The authors would like to thank Dr. Laurent Akrou, Electrochemistry Product Manager at Metrohm France SAS, for his availability and help to improve the electrochemical reactor. In addition, the authors would like to extend their thanks to Dr. Ayadi Hajji for his help with correction, improvement, and proofreading the English of the manuscript.

**Availability of data and materials** Supplementary data is available.

**Author contribution** The contribution of each author is listed as follows:

- ✓ Hana Boubaker: conceptualization, methodology, investigation, writing—original draft, project administration, writing—review and editing, formal analysis, data curation
- ✓ Wafa Sassi: conceptualization, methodology, investigation, writing—original draft, project administration, writing—review and editing, formal analysis, data curation, supervision
- ✓ Hayet Ben-Khaled: experiences, formal analysis, data curation
- ✓ Sana Dhaoui: experiences, formal analysis, data curation
- ✓ Achraf Ghorbal: writing—review and editing, visualization, supervision
- ✓ Jean-Yves Hihn: writing—review and editing, visualization, supervision

## Declarations

**Ethical approval** All the authors deliberately approved the ethical rules adopted by the journal.

**Consent to participate** All the authors expressed their solemn agreement to participate in the conception and elaboration of this work.

**Consent to publish** All the authors deliberately consent to publish this work.

**Competing interests** The authors declare no competing interests.

## References

- Abbas-Ghaleb R, Chlala D, Assaf J-C (2019) Isopropyl alcohol total oxidation over platinum supported on alumina and mullite. *Chem Afr* 2:335–341. <https://doi.org/10.1007/s42250-019-00066-x>
- Amalraj S, Michael PA (2019) Synthesis and characterization of  $\text{Al}_2\text{O}_3$  and  $\text{CuO}$  nanoparticles into nanofluids for solar panel applications. *Results Phys* 15:102797. <https://doi.org/10.1016/j.rinp.2019.102797>
- Araújo CST, Almeida ILS, Rezende HC, Marcionilio SMLO, Léon JJJ, de Matos TN (2018) Elucidation of mechanism involved in

- adsorption of Pb(II) onto lobeira fruit ( *Solanum lycocarpum* ) using Langmuir, Freundlich and Temkin isotherms. *Microchem J* 137: 348–354. <https://doi.org/10.1016/j.microc.2017.11.009>
- Arukula R, Vinothkannan M, Kim AR, Yoo DJ (2019) Cumulative effect of bimetallic alloy, conductive polymer and graphene toward electrooxidation of methanol: an efficient anode catalyst for direct methanol fuel cells. *J Alloys Compd* 771:477–488. <https://doi.org/10.1016/j.jallcom.2018.08.303>
- Ayawei N, Angaye SS, Wankasi D, Dikio ED (2015a) Synthesis, characterization and application of Mg/Al layered double hydroxide for the degradation of Congo red in aqueous solution. *Open J Phys Chem* 05:56–70. <https://doi.org/10.4236/ojpc.2015.53007>
- Ayawei N, Ebelegi AN, Wankasi D (2017) Modelling and interpretation of adsorption isotherms. *J Chemother* 2017:1–11. <https://doi.org/10.1155/2017/3039817>
- Ayawei N, Ekubo AT, Wankasi D, Dikio ED (2015b) Adsorption of Congo red by Ni/Al-CO<sub>3</sub>: equilibrium, thermodynamic and kinetic studies. *Orient J Chem* 31:1307–1318. <https://doi.org/10.13005/oj/310307>
- Baba AA, Olowo VY, Raji MA, Akinribido JP (2020) Preparation of industrial  $\alpha$ -alumina powder from Ijoro Ekiti (Nigeria) Kaolin ore by acid leaching process. *Chem Afr*. <https://doi.org/10.1007/s42250-020-00159-y>
- Balyan S, Sharma R, Lal J (2020) Microwave-assisted, efficient and eco-friendly synthesis of novel 3H-benzo[b][1,4]diazepine derivatives using basic alumina as a reusable catalyst. *Chem Afr* 3:35–44. <https://doi.org/10.1007/s42250-019-00110-w>
- Belaid KD, Kacha S (2011) Étude cinétique et thermodynamique de l'adsorption d'un colorant basique sur la sciure de bois. *Rev Sci L'eau* 24:131–144. <https://doi.org/10.7202/1006107ar>
- Ben-Ali S, Jaouali I, Souissi-Najar S, Ouedemi A (2017) Characterization and adsorption capacity of raw pomegranate peel biosorbent for copper removal. *J Clean Prod* 142:3809–3821. <https://doi.org/10.1016/j.jclepro.2016.10.081>
- Bharath G, Rambabu K, Banat F et al (2019) Enhanced electrochemical performances of peanut shell derived activated carbon and its Fe<sub>3</sub>O<sub>4</sub> nanocomposites for capacitive deionization of Cr(VI) ions. *Sci Total Environ* 691:713–726. <https://doi.org/10.1016/j.scitotenv.2019.07.069>
- Bharath G, Hai A, Rambabu K et al (2020) The fabrication of activated carbon and metal-carbide 2D framework-based asymmetric electrodes for the capacitive deionization of Cr(VI) ions toward industrial wastewater remediation. *Environ Sci Water Res Technol* 6: 351–361. <https://doi.org/10.1039/C9EW00805E>
- Cai C-B, Han Q-J, Tang L-J, Xu L, Jiang JH, Wu HL, Yu RQ (2009) Studying the uptake of aniline vapor by active alumina through in-line monitoring a differential adsorption bed with near-infrared diffuse reflectance spectroscopy. *Adsorption* 15:23–29. <https://doi.org/10.1007/s10450-008-9146-5>
- Chowdhury IH, Kundu S, Naskar MK (2018) Template-free hydrothermal synthesis of MgO-TiO<sub>2</sub> microcubes toward high potential removal of toxic water pollutants. *J Phys Chem Solids* 112:171–178. <https://doi.org/10.1016/j.jpcs.2017.09.021>
- Chu Z, Chen K, Xiao C, Ji D, Ling H, Li M, Liu H (2020) Improving pressure durability and fractionation property via reinforced PES loose nanofiltration hollow fiber membranes for textile wastewater treatment. *J Taiwan Inst Chem Eng* 108:71–81. <https://doi.org/10.1016/j.jtice.2019.12.009>
- Crini G, Lichtfouse E, Wilson L, Morin-Crini N (2018) Adsorption-oriented processes using conventional and non-conventional adsorbents for wastewater treatment. In: *Green Adsorbents for Pollutant Removal*. Springer Nature, pp 23–71
- Crini G, Lichtfouse E, Wilson LD, Morin-Crini N (2019) Conventional and non-conventional adsorbents for wastewater treatment. *Environ Chem Lett* 17:195–213. <https://doi.org/10.1007/s10311-018-0786-8>
- Diao Z-H, Xu X-R, Jiang D, Liu JJ, Kong LJ, Li G, Zuo LZ, Wu QH (2017) Simultaneous photocatalytic Cr(VI) reduction and ciprofloxacin oxidation over TiO<sub>2</sub>/Fe<sub>0</sub> composite under aerobic conditions: Performance, durability, pathway and mechanism. *Chem Eng J* 315: 167–176. <https://doi.org/10.1016/j.cej.2017.01.006>
- Díaz-Sánchez M, Díaz-García D, Prashar S, Gómez-Ruiz S (2019) Palladium nanoparticles supported on silica, alumina or titania: greener alternatives for Suzuki–Miyaura and other C–C coupling reactions. *Environ Chem Lett* 17:1585–1602. <https://doi.org/10.1007/s10311-019-00899-5>
- El-Nahas S, Salman HM, Seleeme WA (2019) Aluminum building scrap wire, take-out food container, potato peels and bagasse as valueless waste materials for nitrate removal from water supplies. *Chem Afr* 2: 143–162. <https://doi.org/10.1007/s42250-018-00032-z>
- Freundlich H (1928) Über die Struktur der Kolloidteilchen und über den Aufbau von Solen und Gelen. *Berichte Dtsch Chem Ges B Ser* 61: 2219–2233. <https://doi.org/10.1002/cber.19280611002>
- Gaikwad MS, Balomajumder C (2018) Removal of Cr(VI) and fluoride by membrane capacitive deionization with nanoporous and microporous Limonia acidissima (wood apple) shell activated carbon electrode. *Sep Purif Technol* 195:305–313. <https://doi.org/10.1016/j.seppur.2017.12.006>
- Gaikwad MS, Balomajumder C, Tiwari AK (2020) Acid treated RHWBAC electrode performance for Cr(VI) removal by capacitive deionization and CFD analysis study. *Chemosphere* 254:126781. <https://doi.org/10.1016/j.chemosphere.2020.126781>
- Guan X-H, Su T, Wang J (2009) Quantifying effects of pH and surface loading on arsenic adsorption on NanoActive alumina using a speciation-based model. *J Hazard Mater* 166:39–45. <https://doi.org/10.1016/j.jhazmat.2008.10.121>
- Guzel P, Aydın YA, Deveci Aksoy N (2016) Removal of chromate from wastewater using amine-based-surfactant-modified clinoptilolite. *Int J Environ Sci Technol* 13:1277–1288. <https://doi.org/10.1007/s13762-016-0954-y>
- Ho Y (2000) The kinetics of sorption of divalent metal ions onto sphagnum moss peat. *Water Res* 34:735–742. [https://doi.org/10.1016/S0043-1354\(99\)00232-8](https://doi.org/10.1016/S0043-1354(99)00232-8)
- Hou H, Shao G, Yang W, Wong W-Y (2020) One-dimensional mesoporous inorganic nanostructures and their applications in energy, sensor, catalysis and adsorption. *Prog Mater Sci* 113:100671. <https://doi.org/10.1016/j.pmatsci.2020.100671>
- Ighalo JO, Ajala OJ, Umenweke G, Ogunniyi S, Adeyanju CA, Igwegbe CA, Adeniyi AG (2020) Mitigation of clofibric acid pollution by adsorption: a review of recent developments. *J Environ Chem Eng* 8:104264. <https://doi.org/10.1016/j.jece.2020.104264>
- Karoui S, Ben Arfi R, Mougin K, Ghorbal A, Assadi AA, Amrane A (2020) Synthesis of novel biocomposite powder for simultaneous removal of hazardous ciprofloxacin and methylene blue: central composite design, kinetic and isotherm studies using Brouers-Sotolongo family models. *J Hazard Mater* 387:121675. <https://doi.org/10.1016/j.jhazmat.2019.121675>
- Kozłowski TT, Pallardy SG (2002) Acclimation and adaptive responses of woody plants to environmental stresses. *Bot Rev* 68:270–334. [https://doi.org/10.1663/0006-8101\(2002\)068\[0270:AAAROW\]2.0.CO;2](https://doi.org/10.1663/0006-8101(2002)068[0270:AAAROW]2.0.CO;2)
- Králik M (2014) Adsorption, chemisorption, and catalysis. *Chem Pap* 68. <https://doi.org/10.2478/s11696-014-0624-9>
- Kumar E, Bhatnagar A, Kumar U, Sillanpää M (2011) Defluoridation from aqueous solutions by nano-alumina: characterization and sorption studies. *J Hazard Mater* 186:1042–1049. <https://doi.org/10.1016/j.jhazmat.2010.11.102>
- Kumari U, Behera SK, Meikap BC (2019) A novel acid modified alumina adsorbent with enhanced defluoridation property: Kinetics, isotherm study and applicability on industrial wastewater. *J Hazard Mater* 365:868–882. <https://doi.org/10.1016/j.jhazmat.2018.11.064>



- Kumari U, Behera SK, Siddiqi H, Meikap BC (2020) Facile method to synthesize efficient adsorbent from alumina by nitric acid activation: batch scale defluorination, kinetics, isotherm studies and implementation on industrial wastewater treatment. *J Hazard Mater* 381: 120917. <https://doi.org/10.1016/j.jhazmat.2019.120917>
- Lamouri S, Hamidouche M, Bouaouadja N, Belhouchet H, Garnier V, Fantozzi G, Trelkat JF (2017) Control of the  $\gamma$ -alumina to  $\alpha$ -alumina phase transformation for an optimized alumina densification. *Bol Soc Esp Cerámica Vidr* 56:47–54. <https://doi.org/10.1016/j.bsecev.2016.10.001>
- Lee SC, Cho MS, Jung SY, Ryu CK, Kim JC (2014) Effects of alumina phases on CO<sub>2</sub> sorption and regeneration properties of potassium-based alumina sorbents. *Adsorption* 20:331–339. <https://doi.org/10.1007/s10450-013-9596-2>
- Li N, Fu F, Lu J, Ding Z, Tang B, Pang J (2017) Facile preparation of magnetic mesoporous MnFe<sub>2</sub>O<sub>4</sub>@SiO<sub>2</sub>-CTAB composites for Cr(VI) adsorption and reduction. *Environ Pollut* 220:1376–1385. <https://doi.org/10.1016/j.envpol.2016.10.097>
- Lin H-T, Venault A, Chang Y (2020) Reducing the pathogenicity of wastewater with killer vapor-induced phase separation membranes. *J Membr Sci* 614:118543. <https://doi.org/10.1016/j.memsci.2020.118543>
- Luo Y, Ding J, Hai J, Tan W, Hao R, Qiu G (2020) Interaction mechanism of dissolved Cr(VI) and manganite in the presence of goethite coating. *Environ Pollut* 260:114046. <https://doi.org/10.1016/j.envpol.2020.114046>
- Marzouk Trifi I, Trifi B, Ben Souissi E, Hamrouni B (2019) Response surface methodology for dyes removal by adsorption onto alginate calcium. *Environ Technol* 41:3473–3482. 1–10. <https://doi.org/10.1080/09593330.2019.1612470>
- Mohammed AA, Khodair ZT, Khadom AA (2020) Preparation, characterization and application of Al<sub>2</sub>O<sub>3</sub> nanoparticles for the protection of boiler steel tubes from high temperature corrosion. *Ceram Int*. <https://doi.org/10.1016/j.ceramint.2020.07.172>
- Mor S, Negi P, Khaiwal R (2018) Assessment of groundwater pollution by landfills in India using leachate pollution index and estimation of error. *Environ Nanotechnol Monit Manag* 10:467–476. <https://doi.org/10.1016/j.enmm.2018.09.002>
- Mor S, Ravindra K, Bishnoi N (2007) Adsorption of chromium from aqueous solution by activated alumina and activated charcoal. *Bioresour Technol* 98:954–957. <https://doi.org/10.1016/j.biortech.2006.03.018>
- Morozova AG, Lonzingier TM, Skotnikov VA, Sahu JN, Mikhailov GG, Schenk JL, Bhattacharyya A, Kapelyushin Y (2020) Utilization of metallurgical slag with presence of novel CaO-MgO-SiO<sub>2</sub>-Al<sub>2</sub>O<sub>3</sub> as a composite sorbent for wastewater treatment contaminated by cerium. *J Clean Prod* 255:120286. <https://doi.org/10.1016/j.jclepro.2020.120286>
- Nie Q, Xie Y, Ma J, Wang J, Zhang G (2020) High piezo-catalytic activity of ZnO/Al<sub>2</sub>O<sub>3</sub> nanosheets utilizing ultrasonic energy for wastewater treatment. *J Clean Prod* 242:118532. <https://doi.org/10.1016/j.jclepro.2019.118532>
- Nordfors D, Ågren H, Mikkelsen KV (1992) The XPS core spectral functions of free and physisorbed molecular oxygen. *Chem Phys* 164:173–182. [https://doi.org/10.1016/0301-0104\(92\)87141-U](https://doi.org/10.1016/0301-0104(92)87141-U)
- Pakade VE, Tavengwa NT, Madikizela LM (2019) Recent advances in hexavalent chromium removal from aqueous solutions by adsorptive methods. *RSC Adv* 9:26142–26164. <https://doi.org/10.1039/C9RA05188K>
- Pils JRV, Laird DA (2007) Sorption of tetracycline and chlortetracycline on K- and Ca-saturated soil clays, humic substances, and clay-humic complexes. *Environ Sci Technol* 41:1928–1933. <https://doi.org/10.1021/es062316y>
- Qiu Y, Zhang Q, Gao B, Li M, Fan Z, Sang W, Hao H, Wei X (2020) Removal mechanisms of Cr(VI) and Cr(III) by biochar supported nanosized zero-valent iron: Synergy of adsorption, reduction and transformation. *Environ Pollut* 265:115018. <https://doi.org/10.1016/j.envpol.2020.115018>
- Romero-González J, Peralta-Videa JR, Rodriguez E et al (2005) Determination of thermodynamic parameters of Cr(VI) adsorption from aqueous solution onto Agave lechuguilla biomass. *J Chem Thermodyn* 37:343–347. <https://doi.org/10.1016/j.jct.2004.09.013>
- Roundhill DM, Koch HF (2002) Methods and techniques for the selective extraction and recovery of oxoanions. *Chem Soc Rev* 31:60–67. <https://doi.org/10.1039/b003141k>
- Sadeghi MH, Tofighy MA, Mohammadi T (2020) One-dimensional graphene for efficient aqueous heavy metal adsorption: rapid removal of arsenic and mercury ions by graphene oxide nanoribbons (GONRs). *Chemosphere* 253:126647. <https://doi.org/10.1016/j.chemosphere.2020.126647>
- Sassi W, Boubaker H, Bahar S, Othman M, Ghorbal A, Zrelli R, Hihn JY (2020a) A challenge to succeed the electroplating of nanocomposite Ni-Cr alloy onto porous substrate under ultrasonic waves and from a continuous flow titanium nanofluids. *J Alloys Compd* 828: 154437. <https://doi.org/10.1016/j.jallcom.2020.154437>
- Sassi W, Msaadi R, Hihn J-Y, Zrelli R (2020b) Effect of pyridine as advanced polymeric inhibitor for pure copper: adsorption and corrosion mechanisms. *Polym Bull*. <https://doi.org/10.1007/s00289-020-03311-3>
- Sassi W, Zrelli R, Hihn J-Y, Berçot P, Rezzazi M, Ammar S (2020c) Silicate dip-coat mechanism as an inhibitor against copper dissolution into alkaline chloride media. *J Bio-Tribo-Corros* 6:50. <https://doi.org/10.1007/s40735-020-00348-9>
- Saxena A, Srivastava AK, Sharma A, Singh B (2009) Kinetics of adsorption of 2-chloroethylethylsulphide on Al<sub>2</sub>O<sub>3</sub> nanoparticles with and without impregnants. *J Hazard Mater* 169:419–427. <https://doi.org/10.1016/j.jhazmat.2009.03.112>
- Seki Y, Seyhan S, Yurdakoc M (2006) Removal of boron from aqueous solution by adsorption on Al<sub>2</sub>O<sub>3</sub> based materials using full factorial design. *J Hazard Mater* 138:60–66. <https://doi.org/10.1016/j.jhazmat.2006.05.033>
- Shahbeig H, Bagheri N, Ghorbanian SA, et al (2013) A new adsorption isotherm model of aqueous solutions on granular activated carbon. 9(4):243–254
- Soliman NK, Moustafa AF (2020) Industrial solid waste for heavy metals adsorption features and challenges: a review. *J Mater Res Technol* 9: 10235–10253. <https://doi.org/10.1016/j.jmrt.2020.07.045>
- Srihari V, Das A (2008) The kinetic and thermodynamic studies of phenol-sorption onto three agro-based carbons. *Desalination* 225: 220–234. <https://doi.org/10.1016/j.desal.2007.07.008>
- Thabede PM, Shooto ND, Xaba T, Naidoo EB (2020) Adsorption studies of toxic cadmium(II) and chromium(VI) ions from aqueous solution by activated black cumin (*Nigella sativa*) seeds. *J Environ Chem Eng* 8:104045. <https://doi.org/10.1016/j.jece.2020.104045>
- Tian J, Tian P, Pang H, Ning G, Bogale RF, Cheng H, Shen S (2016) Fabrication synthesis of porous Al<sub>2</sub>O<sub>3</sub> hollow microspheres and its superior adsorption performance for organic dye. *Microporous Mesoporous Mater* 223:27–34. <https://doi.org/10.1016/j.micromeso.2015.09.055>
- Wakabayashi R, Tomita A, Kimura T (2020) Understanding of NO<sub>x</sub> storage property of impregnated Ba species after crystallization of mesoporous alumina powders. *J Hazard Mater* 398:122791. <https://doi.org/10.1016/j.jhazmat.2020.122791>
- Wan Z, Cho D-W, Tsang DCW, Li M, Sun T, Verpoort F (2019) Concurrent adsorption and micro-electrolysis of Cr(VI) by nanoscale zerovalent iron/biochar/Ca-alginate composite. *Environ Pollut* 247:410–420. <https://doi.org/10.1016/j.envpol.2019.01.047>
- Xing H, Hu P, Li S, Zuo Y, Han J, Hua X, Wang K, Yang F, Feng P, Chang T (2021) Adsorption and diffusion of oxygen on metal surfaces studied by first-principle study: A review. *J Mater Sci Technol* 62:180–194. <https://doi.org/10.1016/j.jmst.2020.04.063>

- Yadav AK, Bhattacharyya S (2019) Preparation of porous alumina adsorbent from kaolin using acid leach method: studies on removal of fluoride toxic ions from an aqueous system. *Adsorption*. <https://doi.org/10.1007/s10450-019-00193-4>
- Yüksel Ş, Orhan R (2019) The removal of Cr(VI) from aqueous solution by activated carbon prepared from apricot, peach stone and almond shell mixture in a fixed-bed column. *Arab J Sci Eng* 44:5345–5357. <https://doi.org/10.1007/s13369-018-3618-z>
- Zhang L, Huang T, Zhang M, Guo X, Yuan Z (2008) Studies on the capability and behavior of adsorption of thallium on nano-Al<sub>2</sub>O<sub>3</sub>. *J Hazard Mater* 157:352–357. <https://doi.org/10.1016/j.jhazmat.2008.01.005>
- Zhang T, Hu L, Zhang M, Jiang M, Fiedler H, Bai W, Wang X, Zhang D, Li Z (2019) Cr(VI) removal from soils and groundwater using an integrated adsorption and microbial fuel cell (A-MFC) technology. *Environ Pollut* 252:1399–1405. <https://doi.org/10.1016/j.envpol.2019.06.051>
- Zhang W, Zhang L, Hua T, Li Y, Zhou X, Wang W, You Z, Wang H, Li M (2020) The mechanism for adsorption of Cr(VI) ions by PE microplastics in ternary system of natural water environment. *Environ Pollut* 257:113440. <https://doi.org/10.1016/j.envpol.2019.113440>

**Publisher's note** Springer Nature remains neutral with regard to jurisdictional claims in published maps and institutional affiliations.